

Grid Impedance Estimation through Grid-Forming Power Converters

Jingyang Fang, *Member, IEEE*, Han Deng, *Student Member, IEEE*, and Stefan M. Goetz, *Member, IEEE*

Abstract—In more-electronics power systems, grid-forming power converters, which operate as ac voltage sources, regulate the grid frequency and voltages in replacement of synchronous generators. Notably, grid impedances greatly influence the small-signal and voltage stability of grid-forming converters. As such, prior knowledge of grid impedances can be very helpful for controller design. However, grid impedance estimation schemes are normally designed for current-controlled grid-following converters. Moreover, they are either very complicated or only yield grid inductances in a generally intrusive way. To fill this research gap, an impedance estimation method well suited to grid-forming converters is proposed. The method consists of four operating modes, which work well in voltage and power control cases. In the voltage control case, the voltage amplitude perturbation or phase angle information is exploited. Subsequently, the grid inductance and resistance are derived from power measurement. Alternatively, the active or reactive power information serves to estimate the grid impedance in the power control case. The proposed method features an easy implementation without any harmonic distortion, safety concern, or dependence on control parameters. Moreover, the method operates non-intrusively in most scenarios. Further, a novel Kalman filtering scheme is proposed to provide added incentives. Finally, simulation and experimental results validate the effectiveness and simplicity of the proposed method.

Index Terms—Grid forming, impedance estimation, Kalman filter, power converter, stability.

I. INTRODUCTION

In modern more-electronics power systems, power electronic converters serve as grid interfaces for renewable generation systems, energy storage systems, electric motor drives, etc. [1]. Generally, grid-tied power converters operate as either ac voltage or current sources, seen from the power grid [2]. Although presently dominant, current-controlled converters lack the ability of grid formation. They simply regulate grid-injected currents and power so as to follow the grid, and thus called grid-following converters [2]. Voltage-controlled or grid-forming converters, in contrast, regulate the amplitudes and frequency of ac voltages. They allow a seamless transition between grid-tied and islanded operation. With respect to grid

synchronization, grid-forming converters and synchronous generators share similar fundamental principles. Therefore, the phase-locked-loop (PLL) is no longer a must after successful grid connection [3]. Because of these attractive features, grid-forming converters gain increasing popularity.

Under grid-tied conditions, grid-forming converters are unavoidably subject to the influence of grid impedances. On the one hand, the nature of grid impedances determines the way of active and reactive power control. Specifically, in the presence of inductive lines, the regulation of ac voltage phase or frequency allows the control of active power, while the reactive power is controlled through the change of voltage amplitudes [4]. However, the opposite is true for resistive lines [5]. On the other hand, grid impedances greatly affect the stability of power converters [6–8]. In this sense, prior knowledge of grid impedance is important for stability.

The stability related to grid impedances is twofold. First, control parameters are generally tuned at the steady-state operating point of power converters so that small-signal stability is guaranteed [9], [10]. Second, the active power transfer capability of power converters depends on grid impedances. In weak grids, which feature large and variable grid inductances, an excessive active power transfer gives rise to large-signal stability problems, e.g., the voltage stability problem [4]. As such, prior knowledge of grid impedances will be highly beneficial for controller design.

Grid impedance estimation approaches are largely classified into two groups, i.e., on-line and off-line approaches. Despite of high accuracy, off-line approaches are not appropriate for real-time applications. Moreover, they typically suffer from high complexity and cost due to the use of additional hardware [11], [12]. Without any additional hardware, grid impedances can be estimated from cable dimensions [13]. Besides compromised accuracy, the calculation approach depends on the availability of cable, grid, and system configuration data.

On-line approaches benefit from fast response and low cost, and hence enjoy growing research interests. Implementations of on-line impedance estimation methods can be further divided into intrusive and non-intrusive (or known as active and passive [11]) approaches. After disturbing power systems, intrusive approaches estimate grid impedances by use of the information obtained from disturbances. For instance, an interharmonic, such as 75 Hz, can be added to the voltage reference of the current control and injected into the network. The resulting 75 Hz current yields the impedance through Fourier analysis [14], [15]. However, the interharmonic causes voltage and current distortions, which must be well treated to comply with grid codes [16]. Moreover, the impedance esti-

Manuscript received October 23, 2019; revised January 14, 2020, April 13, 2020, and June 4, 2020; accepted July 18, 2020. This work was supported by the National Science Foundation under grant No. 1608929.

J. Fang and S. M. Goetz are with Duke University, Durham, NC 27710, USA and Technische Universität Kaiserslautern, Kaiserslautern, RP 67663, Germany (e-mails: jf274@duke.edu or fang@eit.uni-kl.de; stefan.goetz@duke.edu or goetz@eit.uni-kl.de;)

H. Deng is with the School of Electrical and Electronic Engineering, Nanyang Technological University, Singapore 639798 (e-mail: han017@e.ntu.edu.sg)

mation is not very accurate due to time delays and biased disturbance frequencies, and thereby complicating the estimation of grid resistances in experiments [14], [15]. Since the objectives of [14] and [15] are the detection of grid faults, this inaccuracy poses few challenges. However, high accuracy is required for the guidance of controller design. Cespedes and Sun replace the interharmonic by a triangular disturbance, which allows the estimation of grid impedances in a wide bandwidth [17]. However, distortion problems still exist. In fact, the open-loop injection of harmonics or interharmonics, which can interact with converter control, may distort disturbance signals and give incorrect information for grid impedance estimation [18]. One interesting approach estimates the grid impedance via the excitation and detection of *LCL* filter resonances [19]. However, such an approach may destabilize power conversion systems and be safety critical due to resonance amplifications, particularly in the presence of other power converters. Moreover, current controllers affect estimation accuracy, as the resonance is determined by current control gains.

Non-intrusive approaches exploit the existing information in power grids for grid impedance estimation, and hence free of disturbances. As detailed in [20], the extended Kalman filter proves to be a promising tool of estimating grid impedances within several fundamental periods. This approach works well even under distorted environments [21]. However, the extended nonlinear Kalman filter is complicated by large system state-space models and Jacobian matrix calculation. Moreover, the tuning of noise covariance matrices (including measurement and process covariance matrices) are difficult, especially when the number of states is huge. In practice, the tuning is often a trial and error procedure [21]. Therefore, it is highly desirable to simplify system models. In addition, a hybrid approach combining both intrusive and non-intrusive ideas (using recursive least square algorithms) is developed, where disturbances are applied only when the estimation quality falls below a certain limit [22]. However, all these model-based approaches are designed for grid-following converters, and therefore they cannot be directly used in grid-forming converters. Thus, there is a gap in the art, which this paper aims to fill.

This paper proposes an impedance estimation method well suited to grid-forming power converters. The method benefits from easy implementation without any harmonic distortion or safety concern. For stable grid-forming converters, control parameters will not affect impedance detection accuracy. Moreover, the method yields both grid inductances and resistances. The proposed method contains four operating modes, most of which operate non-intrusively without disturbing power systems. The rest of this paper is organized as follows. Section II describes the system configuration and control structure of grid-forming power converters. In Section III, the proposed grid impedance estimation method is disclosed and detailed. Section IV introduces a novel filtering scheme for better noise rejection. Section V verifies the proposed method through extensive simulation and experimental results. Finally, Section V provides the concluding remarks.

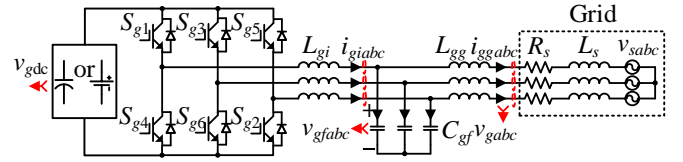


Fig. 1. Schematic diagram of grid-forming power conversion systems.

II. SYSTEM CONFIGURATION AND CONTROL STRUCTURE

This section provides a broad view of system configuration and control structure. The relevant contents lay a foundation for the subsequent descriptions of the proposed grid impedance estimation method.

Fig. 1 shows a schematic diagram of grid-forming power conversion systems, where the dc-ac or ac-dc power converter is connected to the grid through an *LCL* filter. As common practice, we model the grid as a series connection of resistors R_s , inductors L_s , and voltage sources v_{sabc} [20], [22]. The *LCL* filter provides local voltage support through the capacitors C_{gf} , while the grid-side inductors L_{gg} decouple the capacitors from the grid voltages in stiff grids [23]. Dependent on applications, the dc side can contain capacitors or dc voltage sources [24]. The two options differ in the outer active power control loop: with a dc voltage source, the grid-forming converter regulates its active power directly; otherwise, the dc voltage v_{gdc} is controlled, whereas the active power cannot be flexibly regulated. In both cases, the ac capacitor voltages v_{gfabc} should be tightly regulated through a voltage loop inside the dc voltage or power control loop. Moreover, the converter currents or capacitor currents may be sensed for resonance damping and protection purposes [25].

Fig. 2 details the control structure of grid-forming power conversion systems, where PI and P stand for proportional integral and proportional controllers, respectively. LPF represents the low pass filter. d_{abc} serve to generate driving pulses. Noticeably, the voltage control is implemented with a cascaded structure in the synchronous *dq*-frame [2]. The two inputs of voltage control, namely the voltage amplitude v_{gf_ref} ($v_{gf_ref} = V_{gf_ref} + \Delta v_{gf_ref}$) and phase angle δ_{gf_ref} ($\delta_{gf_ref} = \delta_{ref} + \Delta \delta_{gf_ref}$), are determined by the outputs of power control. In particular, δ_{gf_ref} consists of two parts— δ_{ref} (which refers to the phase angle of the grid voltages in steady state) and $\Delta \delta_{gf_ref}$ (which denotes the phase angle difference between the converter voltages and grid voltages in steady state).

Generally, the active power P_g is regulated through the change of its reference P_{g_ref} or phase angle δ_{gf_ref} , while the reactive power Q_g is controlled via its reference Q_{g_ref} or voltage amplitude v_{gf_ref} [26]. However, it is worth noting that this statement holds valid only for inductive grids. For resistive grids, the control philosophy will be opposite [5]. As such, power control is affected by grid impedances. In addition to power control, grid impedances also impact stability and performances of grid-forming power converters [4]. Notably, the knowledge of grid impedances enables the implementation of adaptive controllers, which ensure better ac voltage and power regulation [27]. Moreover, as discussed in [14] and [15], grid

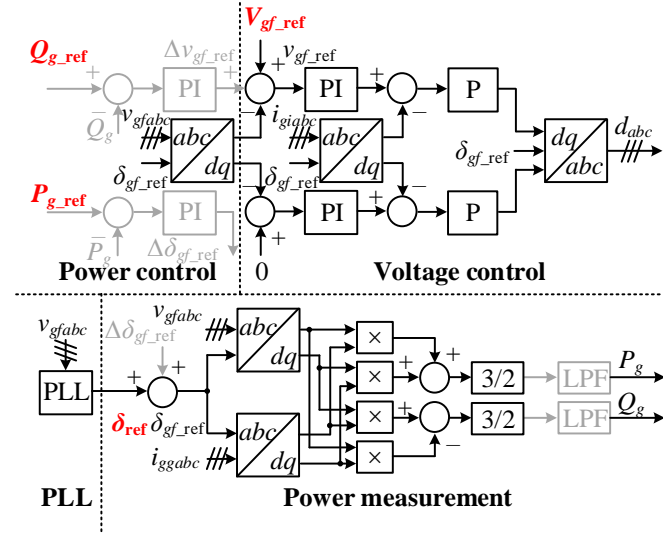


Fig. 2. Control structure of grid-forming power conversion systems.

impedances can predict grid fault and islanding conditions. Also, the successful synchronization of multiple grid-forming converters is determined by grid impedances [31]. Therefore, it is highly desirable to accurately estimate grid impedances, as will be discussed in the following sections.

In Fig. 2, the power measurement part calculates the active power P_g and the reactive power Q_g through the following equations [28]:

$$P_g = \frac{3}{2} (v_{gfd} i_{ggd} + v_{gfq} i_{ggq}), \quad (1)$$

$$Q_g = \frac{3}{2} (v_{gfq} i_{ggd} - v_{gfd} i_{ggq}), \quad (2)$$

where v_{gfd} and v_{gfq} or i_{ggd} and i_{ggq} denote the dq -axis components of v_{gabc} and i_{gabc} , respectively. P_g and Q_g can be filtered by LPFs before sent to the power control part. Prior to grid connection, the PLL synchronizes with grid voltages and provides the phase angle reference δ_{ref} . After successfully connected to the power grid, the grid-forming converter may deactivate its PLL as long as the active power is well regulated.

III. PROPOSED IMPEDANCE ESTIMATION METHOD

This section proposes an impedance estimation method well suited to grid-forming power converters. Also, the theoretical bases and benefits are fully disclosed.

Before proceeding to method details, we can first refer to the simplified circuit diagram shown in Fig. 3(a). Upon achieving a stable grid connection, the grid-forming converter is modeled as a controllable ac voltage source $V_{gf} \angle 0^\circ$, where the capacitor voltage phasor with its phase-to-line voltage amplitude V_{gf} is chosen as a reference of zero degree. The grid current and voltage phasors are represented as $I_{gg} \angle -\phi$ and $V_s \angle -\delta$, respectively. Special attention should be paid to the impedance $Z_{gs} \angle \theta$ connected between the two voltage sources. This impedance is contributed by the grid-side inductance L_{gg} of the LCL filter, the grid resistance R_s , and the grid inductance L_s . $Z_{gs} \angle \theta$ is mathematically described by

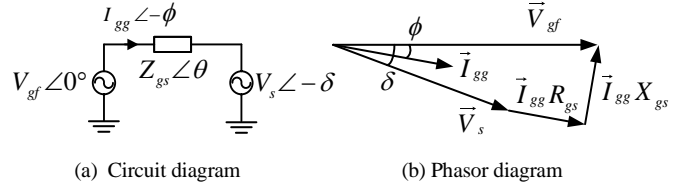


Fig. 3. Simplified schematic diagram for impedance estimation.

$$Z_{gs} \angle \theta = R_{gs} + jX_{gs} = R_s + j\omega_0(L_{gg} + L_s), \quad (3)$$

where ω_0 represents the fundamental angular frequency.

Fig. 3(b) visualizes the relationships among various phasors in Fig. 3(a) through a phasor diagram, from which the grid current phasor is derived as

$$\begin{aligned} \bar{I}_{gg} &= I_{gg} \angle -\phi = \frac{V_{gf} \angle 0^\circ - V_s \angle -\delta}{Z_{gs} \angle \theta} = \frac{V_{gf} - V_s \cos \delta + jV_s \sin \delta}{R_{gs} + jX_{gs}} \\ &= \frac{(V_{gf} - V_s \cos \delta)R_{gs} + V_s \sin \delta X_{gs}}{R_{gs}^2 + X_{gs}^2} + j \frac{[V_s \sin \delta R_{gs} - (V_{gf} - V_s \cos \delta)X_{gs}]}{R_{gs}^2 + X_{gs}^2} \end{aligned} \quad (4)$$

where the complex phasor operations can follow [23].

Further, the active power P_g and the reactive power Q_g injected by the converter to the grid are derived from the complex product of voltage and conjugate current phasors as

$$P_g = \frac{3}{2} \text{Re}(\bar{V}_{gf} \bar{I}_{gg}^*) = \frac{3V_{gf}(V_{gf} - V_s \cos \delta)R_{gs} + 3V_{gf}V_s \sin \delta X_{gs}}{2(R_{gs}^2 + X_{gs}^2)}, \quad (5)$$

$$Q_g = \frac{3}{2} \text{Im}(\bar{V}_{gf} \bar{I}_{gg}^*) = \frac{-3V_{gf}V_s \sin \delta R_{gs} + 3V_{gf}(V_{gf} - V_s \cos \delta)X_{gs}}{2(R_{gs}^2 + X_{gs}^2)}. \quad (6)$$

Assuming that the voltage controller operates normally, the voltage amplitude V_{gf} and phase angle δ are expressed as

$$V_{gf} = v_{gf_ref} = V_{gf_ref} + \Delta v_{gf_ref}, \quad (7)$$

$$\delta = \Delta \delta_{gf_ref}, \quad (8)$$

where V_{gf_ref} ($V_{gf_ref} = V_s$) and δ_{ref} (see Fig. 2) are obtained before grid connection to avoid inrush currents. Moreover, Δv_{gf_ref} and $\Delta \delta_{gf_ref}$ are derived from the controllers in Fig. 2. Therefore, the only unknown information of P_g in (5) and Q_g in (6) is related to the grid impedance, i.e., R_{gs} and X_{gs} . This implies the possibility of using the power measurement information to estimate grid impedances.

A. Amplitude Perturbation in the Voltage Control Case

Generally, grid-forming power converters can operate in either the voltage or power control case. In the voltage control case, the power control part (see Fig. 2) should be ignored. In this case, the converter voltage amplitude v_{gf_ref} and phase angle δ_{gf_ref} are regulated directly. Considering a voltage amplitude perturbation Δv_{gf_ref} and a small phase angle difference, i.e., $\delta \approx 0^\circ$, we can simplify the power expressions (5) and (6) as follows

$$P_g = \frac{3v_{gf_ref} \Delta v_{gf_ref} R_{gs}}{2(R_{gs}^2 + X_{gs}^2)}, \quad (9)$$

$$Q_g = \frac{3v_{gf_ref} \Delta v_{gf_ref} X_{gs}}{2(R_{gs}^2 + X_{gs}^2)}. \quad (10)$$

By use of (9) and (10), it is possible to derive $(P_g^2 + Q_g^2)$, based on which R_{gs} and X_{gs} are further derived as

$$R_{gs} = \frac{3P_g v_{gf_ref} \Delta v_{gf_ref}}{2(P_g^2 + Q_g^2)}, \quad (11)$$

$$X_{gs} = \frac{3Q_g v_{gf_ref} \Delta v_{gf_ref}}{2(P_g^2 + Q_g^2)}. \quad (12)$$

Finally, the grid resistance and inductance are given as

$$R_s = R_{gs}, L_s = X_{gs} / \omega_0 - L_{gg}. \quad (13)$$

Clearly, the voltage amplitude perturbation mode benefits from simplicity. However, its drawback lies in the modification of voltage amplitudes, which may disturb the operation of local loads that are paralleled with filter capacitors.

B. Phase Angle Information in the Voltage Control Case

As mentioned, it is desirable to maintain a standard voltage amplitude in the voltage control mode, i.e., $\Delta v_{gf_ref} = 0$. In this case, the nonzero phase angle information allows the estimation of grid impedances. To validate this statement, the power equations (5) and (6) are changed into

$$P_g = \frac{3v_{gf_ref}^2 (1 - \cos \Delta \delta_{gf_ref}) R_{gs} + 3v_{gf_ref}^2 \sin \Delta \delta_{gf_ref} X_{gs}}{2(R_{gs}^2 + X_{gs}^2)}, \quad (14)$$

$$Q_g = \frac{-3v_{gf_ref}^2 \sin \Delta \delta_{gf_ref} R_{gs} + 3v_{gf_ref}^2 (1 - \cos \Delta \delta_{gf_ref}) X_{gs}}{2(R_{gs}^2 + X_{gs}^2)}. \quad (15)$$

Upon manipulation, the unknown denominators are removed as follows

$$P_g R_{gs} + Q_g X_{gs} = \frac{3v_{gf_ref}^2 (1 - \cos \Delta \delta_{gf_ref})}{2}, \quad (16)$$

$$P_g X_{gs} - Q_g R_{gs} = \frac{3v_{gf_ref}^2 \sin \Delta \delta_{gf_ref}}{2}. \quad (17)$$

Subsequently, R_{gs} and X_{gs} are derived as

$$R_{gs} = \frac{3v_{gf_ref}^2 [(1 - \cos \Delta \delta_{gf_ref}) P_g - \sin \Delta \delta_{gf_ref} Q_g]}{2(P_g^2 + Q_g^2)}, \quad (18)$$

$$X_{gs} = \frac{3v_{gf_ref}^2 [(1 - \cos \Delta \delta_{gf_ref}) Q_g + \sin \Delta \delta_{gf_ref} P_g]}{2(P_g^2 + Q_g^2)}. \quad (19)$$

Despite the involvement of trigonometric operations, the phase angle mode presents a clear advantage from the implementation point of view. It poses no disturbance, and thereby making free operation of grid-forming converters and local loads possible. The voltage control modes discussed in Section III (A) and (B) allow flexible adaptations to various outer power loops, such as P - V and Q - δ control in low voltage grids.

C. Active Power Information in the Power Control Case

Returning to Fig. 2 and considering the power control part without reactive power compensation, one can rearrange the power equations (5) and (6) as

$$P_{g_ref} = \frac{3v_{gf_ref} [(v_{gf_ref} - V_{gf_ref} \cos \Delta \delta_{gf_ref}) R_{gs} + V_{gf_ref} \sin \Delta \delta_{gf_ref} X_{gs}]}{2(R_{gs}^2 + X_{gs}^2)}, \quad (20)$$

$$0 = \frac{3v_{gf_ref} [-V_{gf_ref} \sin \Delta \delta_{gf_ref} R_{gs} + (v_{gf_ref} - V_{gf_ref} \cos \Delta \delta_{gf_ref}) X_{gs}]}{2(R_{gs}^2 + X_{gs}^2)}. \quad (21)$$

Further, it is derived from (21) that

$$R_{gs} = \frac{(v_{gf_ref} - V_{gf_ref} \cos \Delta \delta_{gf_ref}) X_{gs}}{v_{gf_ref} \sin \Delta \delta_{gf_ref}}. \quad (22)$$

Substitution of (22) into (20), it yields

$$P_{g_ref} = \frac{3v_{gf_ref} V_{gf_ref} \sin \Delta \delta_{gf_ref}}{2X_{gs}}. \quad (23)$$

The grid impedance is derived from (22) and (23) as

$$R_{gs} = \frac{3v_{gf_ref} (v_{gf_ref} - V_{gf_ref} \cos \Delta \delta_{gf_ref})}{2P_{g_ref}}, \quad (24)$$

$$X_{gs} = \frac{3v_{gf_ref} V_{gf_ref} \sin \Delta \delta_{gf_ref}}{2P_{g_ref}}, \quad (25)$$

where v_{gf_ref} and $\Delta \delta_{gf_ref}$ are given in Fig. 2.

It is worthwhile to note that the active power information for impedance estimation comes from the active power reference P_{g_ref} instead of active power measurement. Moreover, the active power method estimates grid impedances using the existing converter information without any disturbance.

D. Reactive Power Information in the Power Control Case

When compensating reactive power, the grid-forming converter operates as a distribution static compensator (DSTAT-COM) [29]. The corresponding power equations take the form of

$$0 = \frac{3v_{gf_ref} [(v_{gf_ref} - V_{gf_ref} \cos \Delta \delta_{gf_ref}) R_{gs} + V_{gf_ref} \sin \Delta \delta_{gf_ref} X_{gs}]}{2(R_{gs}^2 + X_{gs}^2)}, \quad (26)$$

$$Q_{g_ref} = \frac{3v_{gf_ref} [-V_{gf_ref} \sin \Delta \delta_{gf_ref} R_{gs} + (v_{gf_ref} - V_{gf_ref} \cos \Delta \delta_{gf_ref}) X_{gs}]}{2(R_{gs}^2 + X_{gs}^2)}. \quad (27)$$

Rearranging (26) entails

$$R_{gs} = \frac{-V_{gf_ref} \sin \Delta \delta_{gf_ref} X_{gs}}{v_{gf_ref} - V_{gf_ref} \cos \Delta \delta_{gf_ref}}. \quad (28)$$

Substitution of (28) into (27) gives

$$Q_{g_ref} = \frac{-3v_{gf_ref} V_{gf_ref} \sin \Delta \delta_{gf_ref}}{2R_{gs}}. \quad (29)$$

The combination of (28) and (29) yields

$$R_{gs} = \frac{-3v_{gf_ref} V_{gf_ref} \sin \Delta \delta_{gf_ref}}{2Q_{g_ref}}, \quad (30)$$

$$X_{gs} = \frac{3v_{gf_ref} (v_{gf_ref} - V_{gf_ref} \cos \Delta \delta_{gf_ref})}{2Q_{g_ref}}. \quad (31)$$

Similar to the active power mode, the reactive power mode involves no disturbance or power measurement information.

Note that the proposed impedance estimation method cannot differentiate the change of grid impedances when grid voltages also change, because impedance and/or grid voltage changes may lead to identical active and reactive power changes. In this case, we have to reduce the power references to zero. Subsequently, the information of grid voltages can be read from converter voltages. Otherwise, if the change of grid voltages is relatively small as compared to converter power ratings, the errors of the estimated grid impedance will be minor, and hence ignored. In summary, the impedance estimation method containing four operating modes introduced in this section are well suitable for grid-forming converters. They use the steady-state power information for impedance estimation, and hence independent of control parameters. The estimation results cover both the grid resistance and inductance.

IV. PROPOSED KALMAN FILTERING SCHEME

A major limitation of many methods in real-world environments is measurement and interference noise. We propose an advanced filtering scheme that improves the noise rejection performances of our grid impedance estimation. Our proposed method defines a state space to recursively estimate the grid impedance based on the more general concept of Kalman filters [21], [30].

Among Kalman filters, basic and extended Kalman filters are popular choices that target at linear and nonlinear problems, respectively [21]. In contrast, extended Kalman filters are more complicated due to the calculation of Jacobian matrices. Therefore, it is preferable to use basic Kalman filters in replacement of extended Kalman filters if possible.

Fig. 4 illustrates a flowchart of the proposed Kalman filtering scheme, where the process works in two recursive steps, i.e., prediction and update. In Fig. 4, the subscript k stands for the discrete time step. \mathbf{A}_k , \mathbf{B}_k , and \mathbf{H}_k designate the state, input, and output matrices, respectively. \mathbf{x}_k or \mathbf{x}_{k+1} , \mathbf{u}_k , and \mathbf{y}_k represent the real state, input, and output variables, respectively. $\hat{\mathbf{x}}_{k|k-1}$ and $\hat{\mathbf{x}}_k$ denote the prediction and update of \mathbf{x}_k , respectively. \mathbf{K}_k , $\mathbf{P}_{k|k-1}$, and \mathbf{P}_k stand for the Kalman gain, estimate error covariance, and updated error covariance, respectively.

Heightened attention should be paid to the process and measurement noise covariance matrices \mathbf{Q}_k and \mathbf{R}_k , as they are difficult to design in real-time applications, particularly for the systems with a large number of state variables [20]. For exam-

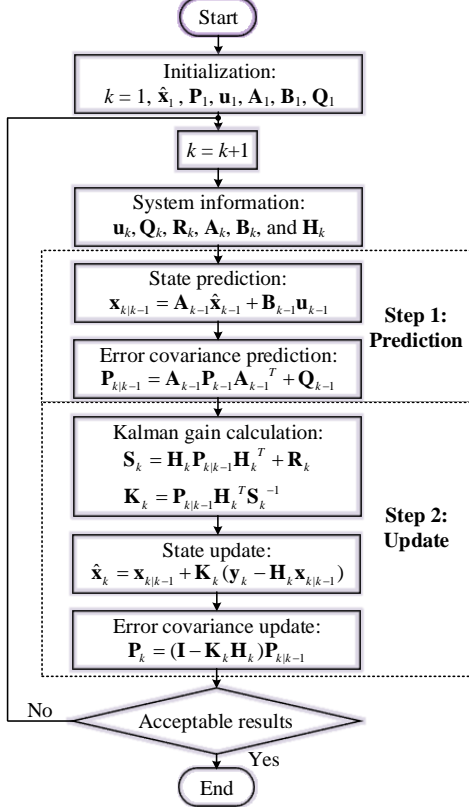


Fig. 4. Flowchart of the proposed Kalman filtering scheme.

ple, the full-order state space model of grid-following converters introduces $\mathbf{Q}_k(14 \times 14)$ and $\mathbf{R}_k(4 \times 4)$, which are very difficult to tune due to high matrix dimensions [20]. Therefore, we aim to simplify system models with less state variables.

First of all, a discrete state-space description of (5) and (6) is given as

$$\begin{aligned} \mathbf{x}_{k+1} &= \mathbf{A}_k \mathbf{x}_k \\ \mathbf{y}_k &= \mathbf{H}_k \mathbf{x}_k + \mathbf{v}_k \end{aligned}, \quad (32)$$

where \mathbf{v}_k refers to the unknown random variable that models the measurement noise. The remaining vectors and matrices are derived as

$$\mathbf{x}_k = \begin{bmatrix} x_{1k}(k) \\ x_{2k}(k) \end{bmatrix} = \begin{bmatrix} R_{gs}(k) \\ R_{gs}(k)^2 + X_{gs}(k)^2 \\ X_{gs}(k) \\ R_{gs}(k)^2 + X_{gs}(k)^2 \end{bmatrix}, \mathbf{y}_k = \begin{bmatrix} P_g(k) \\ Q_g(k) \end{bmatrix}, \quad (33)$$

$$\mathbf{A}_k = \mathbf{A} = \begin{bmatrix} 1 & 0 \\ 0 & 1 \end{bmatrix}, \mathbf{H}_k = \begin{bmatrix} H_{11}(k) & H_{12}(k) \\ -H_{12}(k) & H_{11}(k) \end{bmatrix}, \quad (34)$$

where the coefficients of \mathbf{H}_k are expressed as

$$\begin{aligned} H_{11}(k) &= \frac{3v_{gf_ref}(k)[v_{gf_ref}(k) - V_{gf_ref} \cos \Delta \delta_{gf_ref}(k)]}{2} \\ H_{12}(k) &= \frac{3v_{gf_ref}(k)V_{gf_ref} \sin \Delta \delta_{gf_ref}(k)}{2} \end{aligned}. \quad (35)$$

Note that all the variables in (32)–(35) are discretized to facilitate the recursive process. In addition, the proposed filtering scheme is of a second-order model, which is linear and much simpler than the full-order state space model described in [20].

Next, the initialization is achieved by randomly designing $\hat{\mathbf{x}}_1$ and \mathbf{P}_1 , such as a zero vector and an identity matrix. It should be remembered that the input vector \mathbf{u}_k and input matrix \mathbf{B}_k are excluded from the proposed filter. Moreover, the noise covariance matrices $\mathbf{Q}_k(2 \times 2)$ and $\mathbf{R}_k(2 \times 2)$ can be simplified as constant matrices $\mathbf{Q}(2 \times 2)$ and $\mathbf{R}(2 \times 2)$. This simplification, along with the reduced system order, greatly eases the tuning of the noise covariance matrices.

In what follows, the two steps in Fig. 4, i.e., prediction and update, are alternately performed to yield more accurate estimation of \mathbf{x}_k through $\hat{\mathbf{x}}_k$. Finally, the grid resistance and reactance are derived as

$$R_{gs}(k) = \frac{x_{1k}(k)}{x_{1k}(k)^2 + x_{2k}(k)^2}, X_{gs}(k) = \frac{x_{2k}(k)}{x_{1k}(k)^2 + x_{2k}(k)^2}. \quad (36)$$

The proposed filtering scheme achieves the mitigation of measurement noises for grid impedance estimation methods in a very simple way. It gets rid of the large system state-space models and Jacobian matrix calculation. The filtering effectiveness will be demonstrated in the next section.

V. SIMULATION AND EXPERIMENTAL VERIFICATIONS

We perform simulation and experimental studies in this section for verification purposes. The simulation and experi-

TABLE I. System parameters of grid-forming power conversion systems.

Descriptions	Symbols	Values
Fundamental frequency	f_0	50 Hz
Sampling/switching frequency	f_s/f_{sw}	10 kHz
Nominal dc voltage	V_{gdc}	400 V
Nominal grid voltage	V_{gf_ref}	110 Vrms
Converter-side inductance	L_{gi}	2 mH
Filter capacitance	C_{gf}	40 μ F
Grid-side inductance	L_{gg}	5 mH
Grid resistance	R_s	1/10 Ω
Grid inductance	L_s	10/5 mH

TABLE II. Control parameters of grid-forming power conversion systems.

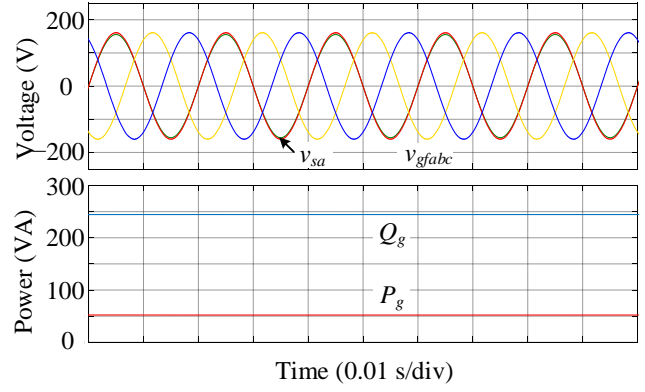
Descriptions	Symbols	Values
Current control gain	K_{ep}	1
Voltage control P gain	K_{vp}	0.2
Voltage control I gain	K_{vi}	70
Active power control P gain	K_{pp}	0
Active power control I gain	K_{pi}	0.01
Reactive power control P gain	K_{qp}	0
Reactive power control I gain	K_{qi}	0.01
Process covariance matrix	$\mathbf{Q}_{(2 \times 2)}$	[1e-3 0; 0 1e-3]
Measurement covariance matrix	$\mathbf{R}_{(2 \times 2)}$	[1e8 0; 0 1e8]
LPF cut-off frequency	f_c	20 Hz
Voltage amplitude perturbation	Δv_{gf_ref}	5 V
Phase angle change	$\Delta \delta_{gf_ref}$	5°
Nominal active power	P_{g_ref}	100 W
Nominal reactive power	Q_{g_ref}	100 Var

mental results clearly verify the effectiveness of the proposed grid impedance estimation method and filtering scheme.

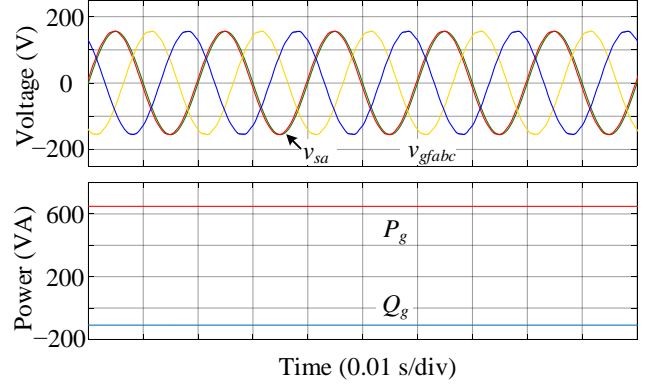
A. Simulation Verification

We simulated the system in Matlab/Simulink (R2016b) with the system and control parameters in Tables I and II, respectively. As noted in Table I, the simulation covers two grid conditions, where the theoretical grid resistance and inductance are 1 Ω and 10 mH as well as 10 Ω and 5 mH, respectively. In Table II, the process covariance matrix, namely, $\mathbf{Q}_{(2 \times 2)}$, is tuned as an identity matrix scaled by a small gain factor 1e-3. We choose a small gain for $\mathbf{Q}_{(2 \times 2)}$ as the filter model in (32) contains no input or input process noise. Alternatively, $\mathbf{R}_{(2 \times 2)}$ features a relatively large gain factor of 1e8, which aims to sufficiently attenuate the measurement noise.

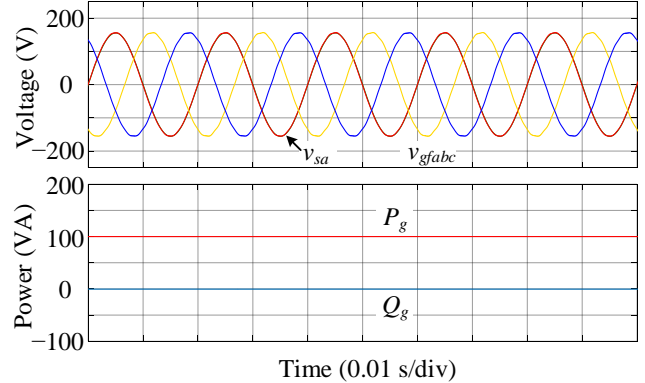
Fig. 5 illustrates the simulated voltage (v_{gfabc} and v_{sa}) and power (P_g and Q_g) waveforms of the proposed grid impedance estimation method under nominal operating conditions. One can notice a small difference between the converter and grid voltage amplitudes in the amplitude perturbation mode. Similarly, there is a phase shift between the converter and grid voltages when the phase angle mode is applied. However, the



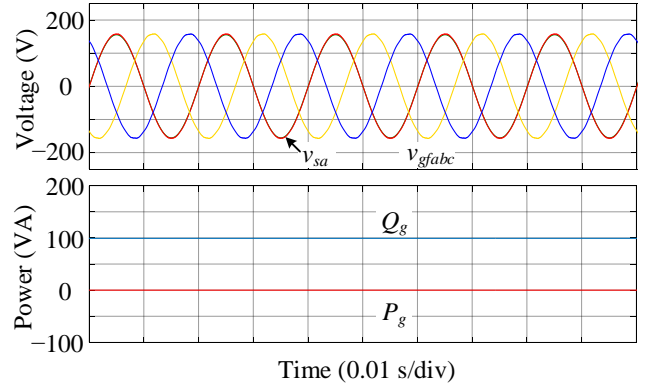
(a) Amplitude perturbation mode



(b) Phase angle mode



(c) Active power mode

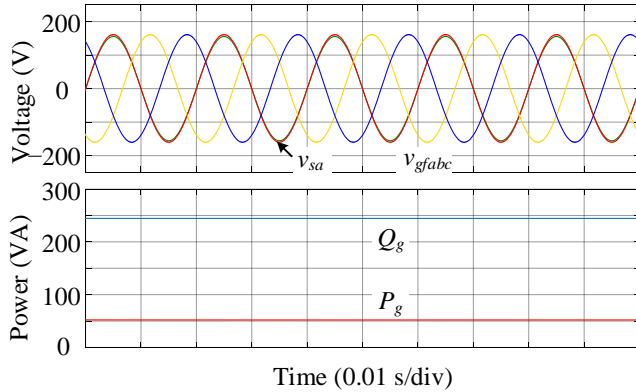


(d) Reactive power mode

Fig. 5. Simulation waveforms of the proposed grid impedance estimation method under nominal operating conditions.

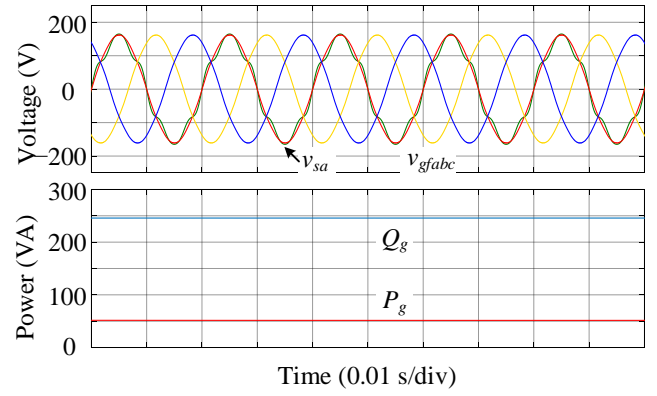
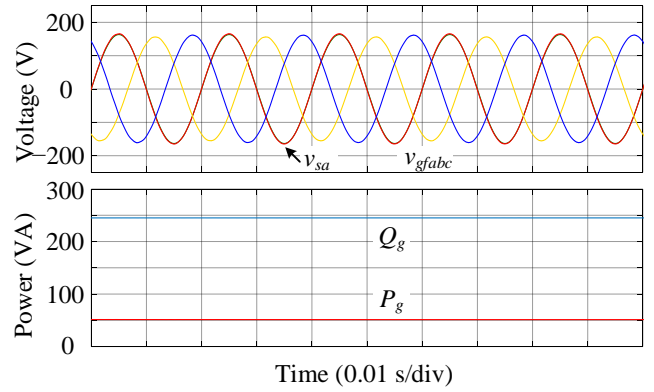
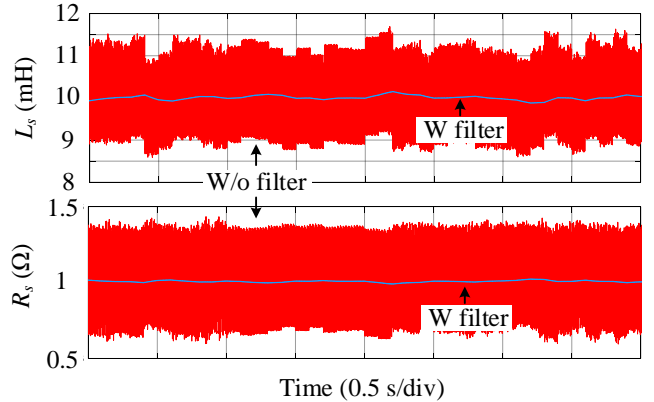
TABLE III. Simulation results of grid impedance estimation.

Cases		R_s (Ω)	L_{gs} (mH)
Nominal case	Theory	1/10	10/5
	Voltage amplitude	1.01/10.0	10.0/4.97
	Phase angle	1.00/10.0	10.0/5.00
	Active power	1.00/9.99	10.0/5.04
	Reactive power	1.00/10.0	10.0/4.98
With 50 Ω local loads	Theory	1/10	10/5
	Voltage amplitude	1.01/10.0	10.0/4.98
	Phase angle	1.01/10.0	10.0/5.00
	Active power	1.00/9.99	9.99/5.03
With voltage harmonics	Theory	1/10	10/5
	Voltage amplitude	1.00/10.0	10.0/4.99
	Phase angle	1.01/10.0	10.0/4.97
	Active power	1.00/10.0	10.1/5.03
With voltage imbalances	Theory	1/10	10/5
	Voltage amplitude	0.99/10.0	9.99/5.04
	Phase angle	1.00/10.0	10.0/5.00
	Active power	0.98/10.0	10.1/5.10
	Reactive power	0.96/9.99	9.95/5.02


Fig. 6. Simulation waveforms of the proposed grid impedance estimation method with 50 Ω local loads.

voltage amplitude and phase angle differences are quite small, thereby demonstrating the high resolution of the proposed grid impedance estimation method. Moreover, the active or reactive power is tightly regulated after enabling the power controller in Fig. 5(c) and (d). In summary, all the proposed modes yield accurate estimation of the grid resistance and inductance, as listed in Table III.

We provide the simulation results under various operating conditions of grid-forming power conversion systems, where only the waveforms associated with the voltage amplitude mode are included for simplicity. Figs. 6–8 present the simulation waveforms of voltages and power with 50 Ω local loads, 10% 5th + 4% 7th grid harmonics, and 5% grid voltage imbalances, respectively. The relevant results are given in Table III.


Fig. 7. Simulation waveforms of the proposed grid impedance estimation method with 10% 5th + 4% 7th grid harmonics.

Fig. 8. Simulation waveforms of the proposed grid impedance estimation method with 5% grid imbalances.

Fig. 9. Simulation results of the proposed filtering scheme.

Despite minor estimation errors, the estimated grid impedances are very close to their theoretical values, thereby demonstrating the effectiveness of the proposed impedance estimation method under various system conditions.

Fig. 9 visualizes the performance of the proposed filtering scheme in the presence of measurement noise. Clearly, the proposed filtering scheme ensures successful estimation despite of noise. It is worth mentioning that the noise rejection performance of filters is strongly related to the measurement

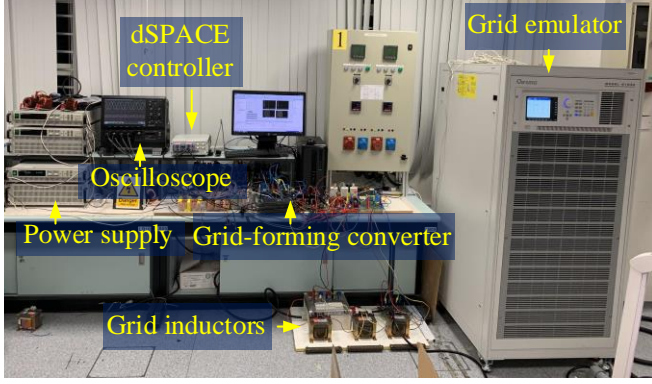


Fig. 10. Photo of experimental setup.

TABLE VI. Experimental setup descriptions.

Equipment	Models	Descriptions
Dc power supply	ITECH IT6536D	750 V/30 A
Controller	DSPACE Microlabbox	48 PWM + 32 AD
Oscilloscope	LeCroy HDO8038	350 MHz, 8 channels
Current probe	LeCroy CP030	50 MHz, 30 A
Voltage probe	LeCroy HVD3106	120 MHz, 1 kV
Grid emulator	Chroma 61830	30 kVA, 4 quadrants
SiC MOSFET	CREE C3M0065090D	900 V, 36 A

covariance matrix $\mathbf{R}_{(2 \times 2)}$. Generally, a larger norm of $\mathbf{R}_{(2 \times 2)}$ translates into better noise rejection at the expense of filtering dynamics.

B. Experimental Verification

We conducted experiments for further verification purposes, where the nominal dc and grid voltage are reduced to 200 V and 50 Vrms, respectively. The method intends to estimate the inductance and equivalent series resistance of discrete grid inductors ($15 \text{ mH} \pm 10\%$).

Fig. 10 presents a photo of the experimental setup, and the detailed experimental setup descriptions are documented in Table VI. A grid emulator (Chroma 61830) together with the grid inductors emulated the power grid. The grid-forming converter was fed by one dc power supply (ITECH IT6536D) and employed SiC MOSFETs (CREE C3M0065090D) as main active switches, which were controlled by a dSPACE microprocessor (Microlabbox). An oscilloscope (LeCroy HDO8038) captured all the experimental waveforms.

Fig. 11 illustrates the experimental waveforms of the proposed grid impedance estimation method under nominal operating conditions. Further, Figs. 12–14 present the relevant experimental waveforms in the cases with local loads, grid voltage harmonics, and grid voltage imbalances, respectively. These experimental results agree well with the simulation results. Nevertheless, the converter and grid voltages, paired with their active and reactive power, are changed in values according to various system operating points.

The estimated grid resistances and inductances are listed in Table V. It is noticed that the estimation errors are slightly magnified as compared to the simulation results. However, the

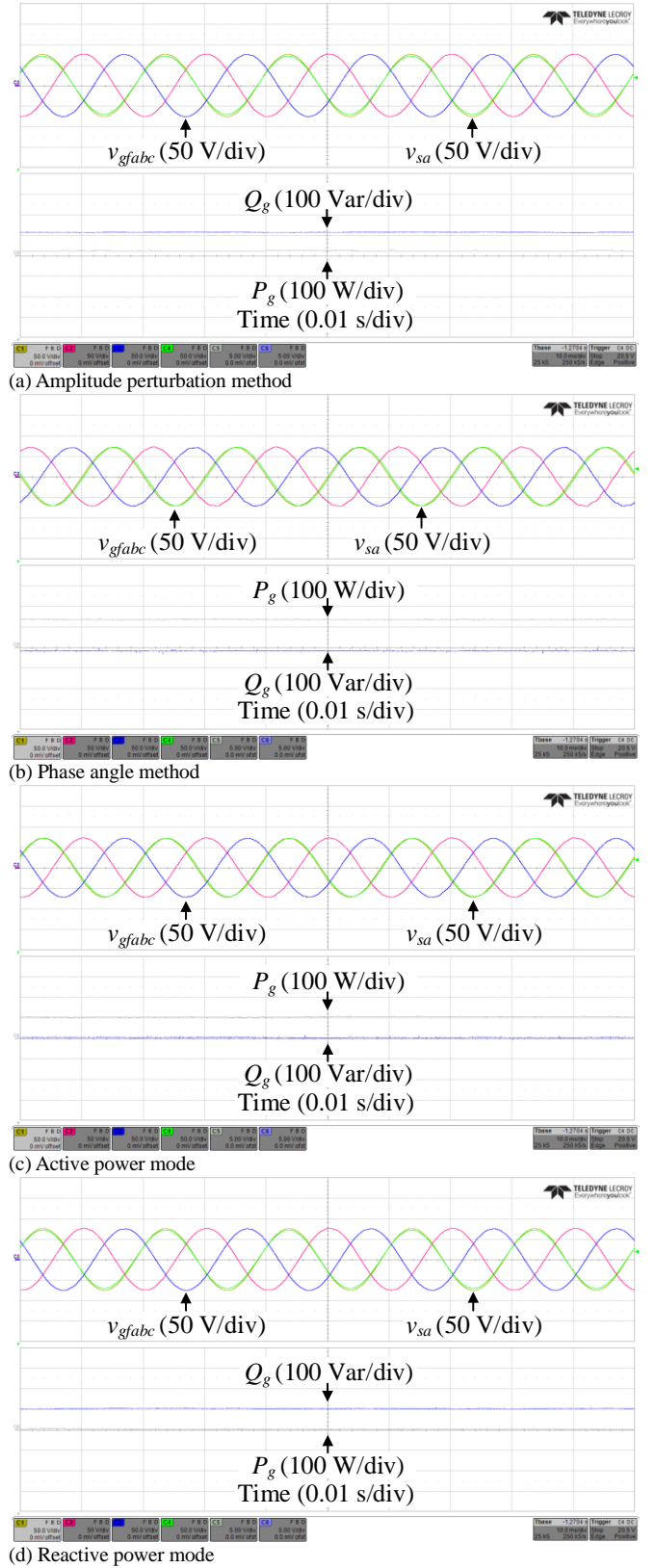


Fig. 11. Experimental waveforms of the proposed grid impedance estimation method under nominal operating conditions.

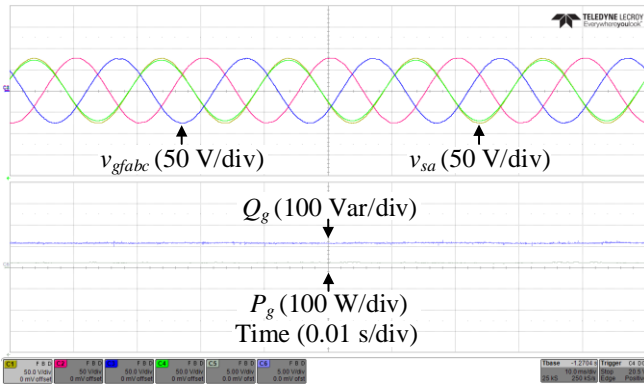


Fig. 12. Experimental waveforms of the proposed grid impedance estimation method with 50 Ω local loads.

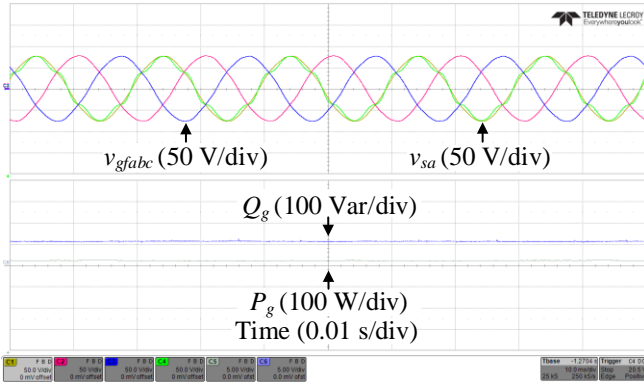


Fig. 13. Experimental waveforms of the proposed grid impedance estimation method with 10% 5th + 4% 7th grid harmonics.

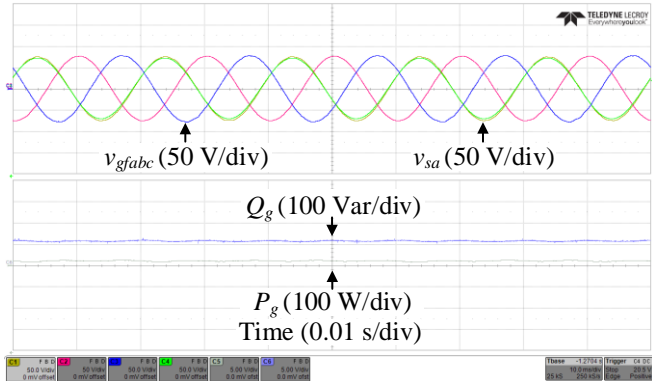


Fig. 14. Experimental waveforms of the proposed grid impedance estimation method with 5% grid imbalances.

errors are within 5% and 10% concerning the grid inductance and resistance, respectively. One possible source of errors lies in the power measurement, particularly for the reactive power measurement. Referring to Table V, one can observe that the voltage amplitude and reactive power modes yield more relatively unreliable results, which are caused by large reactive power ratings in these cases.

Finally, Fig. 15 shows the experimental results of the proposed filtering scheme. The Kalman filter sufficiently attenuates the noise, resulting in clear and readable grid impedance results. These experimental results clearly demonstrate the

TABLE V. Experimental results of grid impedance estimation.

Cases		R_s (Ω)	L_{gs} (mH)
Nominal case	Theory	≈ 0.95	≈ 15.5
	Voltage amplitude	0.90	15.9
	Phase angle	0.93	15.3
	Active power	0.97	15.2
With 50 Ω local loads	Theory	≈ 0.95	≈ 15.5
	Voltage amplitude	0.95	15.9
	Phase angle	0.99	15.2
	Active power	0.91	15.2
With voltage harmonics	Theory	≈ 0.95	≈ 15.5
	Voltage amplitude	0.91	16.0
	Phase angle	0.97	15.4
	Active power	0.94	15.3
With voltage imbalances	Theory	≈ 0.95	≈ 15.5
	Voltage amplitude	0.91	15.8
	Phase angle	0.94	15.4
	Active power	0.92	15.4
	Reactive power	0.83	15.8

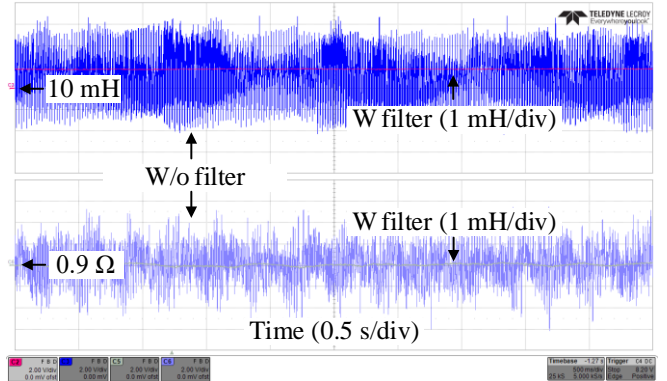


Fig. 15. Experimental results of the proposed filtering scheme.

effectiveness and benefits of the proposed grid impedance estimation method and filtering scheme.

VI. CONCLUSIONS

This paper has proposed a grid impedance estimation method for grid-forming power converters. The proposed method can be easily implemented and applied to various system operating conditions. Specifically, in the voltage control mode, either the voltage amplitude perturbation or the phase angle information, together with the measured active and reactive power, serves to estimate grid impedances. Alternatively, a non-intrusive estimation is achieved by use of active or reactive power information in the power control mode. The proposed method yields both grid inductances and resistances,

without introducing harmonic distortion. Further, we designed a Kalman filtering scheme for better noise rejection. The proposed filtering scheme features a simplified system model and an easy tuning process. Simulation and experimental results clearly demonstrate the effectiveness of the proposed method. Upon the successful estimation of grid impedances, the controller design and stability analysis of grid-forming converters become much easier. The proposed grid impedance estimation method can be adapted and extended to grid-following power converters.

REFERENCES

- [1] F. Blaabjerg, R. Teodorescu, M. Liserre, and A. V. Timbus, "Overview of control and grid synchronization for distributed power generation systems," *IEEE Trans. Ind. Electron.*, vol. 53, no. 5, pp. 1398–1409, Oct. 2006.
- [2] J. Rocabert, A. Luna, F. Blaabjerg, and P. Rodríguez, "Control of power converters in AC microgrids," *IEEE Trans. Power Electron.*, vol. 27, pp. 4734–4749, Nov. 2012.
- [3] Q.-C. Zhong, P.-L. Nguyen, Z. Ma, and W. Sheng, "Self-synchronized synchronverters: inverters without a dedicated synchronization unit," *IEEE Trans. Power Electron.*, vol. 29, no. 2, pp. 617–630, Feb. 2014.
- [4] P. Kundur, *Power system stability and control*. New York, NY, USA: McGraw-Hill, 1994.
- [5] K. De Brabandere, B. Bolsens, J. Van den Keybus, A. Woyte, J. Driesen, and R. Belmans, "A voltage and frequency droop control method for parallel inverters," *IEEE Trans. Power Electron.*, vol. 22, pp. 1107–1115, Jul. 2007.
- [6] M. Liserre, R. Teodorescu, and F. Blaabjerg, "Stability of photovoltaic and wind turbine grid-connected inverters for a large set of grid impedance values," *IEEE Trans. Power Electron.*, vol. 21, pp. 263–272, Jan. 2006.
- [7] J. Fang, P. Lin, H. Li, Y. Yang, and Y. Tang, "An improved virtual inertia control for three-phase voltage source converters connected to a weak grid," *IEEE Trans. Power Electron.*, vol. 34, no. 9, pp. 8660–8670, Sep. 2019.
- [8] V. Natarajan and G. Weiss, "Synchronverters with better stability due to virtual inductors, virtual capacitors, and anti wind-up," *IEEE Trans. Ind. Electron.*, vol. 64, no. 7, pp. 5994–6004, Jul. 2017.
- [9] R. D. Middlebrook, "Input filter considerations in design and application switching regulators," in *Proc. IEEE Ind. Appl. Soc.*, 1976, pp. 366–382.
- [10] J. Sun, "Small-signal methods for AC distributed power systems—a review," *IEEE Trans. Power Electron.*, vol. 24, no. 11, pp. 2545–2554, Nov. 2009.
- [11] J. P. Rhode, A. W. Kelley, and M. E. Baran, "Complete characterization of utilization-voltage power system impedance using wideband measurement," *IEEE Trans. Ind. Appl.*, vol. 33, no. 6, pp. 1472–1479, Nov./Dec. 1997.
- [12] M. Sumner, B. Palethorpe, D. W. P. Thomas, P. Zanchetta, and M. C. D. Piazza, "A technique for power supply harmonic impedance estimation using a controlled voltage disturbance," *IEEE Trans. Power Electron.*, vol. 17, no. 2, pp. 207–215, Mar. 2002.
- [13] U. Borup, B. V. Nielsen, and F. Blaabjerg, "Compensation of cable voltage drops and automatic identification of cable parameters in 400 Hz ground power units," *IEEE Trans. Ind. Appl.*, vol. 40, no. 5, pp. 1281–1286, Sep./Oct. 2004.
- [14] L. Asiminoaei, R. Teodorescu, F. Blaabjerg, and U. Borup, "A digital controlled PV-inverter with grid impedance estimation for ENS detection," *IEEE Trans. Power Electron.*, vol. 20, no. 6, pp. 1480–1490, Nov. 2005.
- [15] A. V. Timbus, R. Teodorescu, F. Blaabjerg, and U. Borup, "Online grid measurement and ENS detection for PV inverter running on highly inductive grid," *IEEE Power Electron. Lett.*, vol. 2, no. 3, pp. 77–82, Sep. 2004.
- [16] *IEEE recommended practices and requirements for harmonic control in electric power systems*, IEEE Standard 519-2014, 2014.
- [17] M. Cespedes and J. Sun, "Online grid impedance identification for adaptive control of grid-connected inverters," in *Proc. Energy Convers. Cong. Expo.*, Sep. 15–20, 2012, pp. 914–921.
- [18] X. Wang, L. Harnefors, and F. Blaabjerg, "Unified impedance model of grid-connected voltage-source converters," *IEEE Trans. Power Electron.*, vol. 33, no. 2, pp. 1775–1787, Feb. 2018.
- [19] M. Liserre, F. Blaabjerg, and R. Teodorescu, "Grid impedance estimation via excitation of LCL-filter resonance," *IEEE Trans. Ind. Appl.*, vol. 43, no. 5, pp. 1401–1407, Sep./Oct. 2007.
- [20] N. Hoffmann, and F. W. Fuchs, "Minimal invasive equivalent grid impedance estimation in inductive–resistive power networks using extended Kalman filter," *IEEE Trans. Power Electron.*, vol. 29, no. 2, pp. 631–641, Feb. 2014.
- [21] G. Welch and G. Bishop, "An Introduction to the Kalman Filter," Univ. North Carolina, Chapel Hill, USA, Tech. Rep. TR 95-041, 2004.
- [22] S. Cobrecas, E. J. Bueno, D. Pizarro, F. J. Rodriguez, and F. Huerta, "Grid impedance monitoring system for distributed power generation electronic interfaces," *IEEE Trans. Instrum. Meas.*, vol. 58, no. 9, pp. 3112–3121, Sep. 2009.
- [23] J. W. Nilsson and S. A. Riedel, *Electric circuits (10th edition)*. New Jersey, NJ, USA: Prentice Hall, 2015.
- [24] J. Fang, H. Li, Y. Tang, and F. Blaabjerg, "On the inertia of future more-electronics power systems," *IEEE J. Emerg. Sel. Topics Power Electron.*, vol. 7, no. 4, pp. 2130–2146, Dec. 2019.
- [25] P. C. Loh and D. G. Holmes, "Analysis of multiloop control strategies for LC/CL/LCL-filtered voltage-source and current-source inverters," *IEEE Trans. Ind. Appl.*, vol. 43, no. 5, pp. 1401–1407, Sep./Oct. 2007.
- [26] J. A. Suul, S. D'Arco, and G. Guidi, "Virtual synchronous machinebased control of a single-phase bi-directional battery charger for providing vehicle-to-grid services," *IEEE Trans. Ind. Appl.*, vol. 52, no. 4, pp. 3234–3244, Jul./Aug. 2016.
- [27] J. Fang, J. Yu, Y. Zhang, and S. M. Goetz, "An estimation-based solution to weak-grid-induced small-signal stability problems of power converters," *IEEE Trans. Power Electron.*, under review.
- [28] H. Akagi, Y. Kanazawa, and A. Nabae, "Instantaneous reactive power compensators comprising switching devices without energy storage components," *IEEE Trans. Ind. Appl.*, vol. 20, no. 3, pp. 625–630, May/Jun. 1984.
- [29] B. Singh, P. Jayaprakash, D. P. Kothari, A. Chandra, and K. A. Haddad, "Comprehensive study of DSTATCOM configurations," *IEEE Trans. Ind. Inform.*, vol. 10, no. 2, pp. 854–870, May. 2014.
- [30] R. E. Kalman, "A new approach to linear filtering and prediction problems," *Trans. ASME J. Basic Eng.*, vol. 82, pp. 34–45, Mar. 1960.
- [31] F. Dorfler, J. W. Simpson-Porco, and F. Bullo, "Electrical networks and algebraic graph theory: Models, properties, and applications," *Proceedings of the IEEE*, vol. 106, no. 5, pp. 977–1005, 2018.



Jingyang Fang (S'15-M'19) received the B.Sc. and M.Sc. degrees in electrical engineering from Xi'an Jiaotong University, Xi'an, China, in 2013 and 2015, respectively, and the Ph.D. degree from School of Electrical and Electronic Engineering, Nanyang Technological University, Singapore, in 2019.

From May 2018 to August 2018, he was a Visiting Scholar with the Institute of Energy Technology, Aalborg University, Aalborg, Denmark. From August 2018 to August 2019, he was a Research Fellow with the School of Electrical and Electronic Engineering, Nanyang Technological University, Singapore. Since August 2019, he joined the Duke University and TU Kaiserslautern as a postdoctoral fellow. His research interests include power quality control, stability analysis and improvement, renewable energy integration, and digital control in more-electronics power systems.

Dr. Fang is the recipient of the Best Paper Award of IEEE Asia Conference on Energy, Power and Transportation Electrification (ACEPT) in 2017 and the Best presenter of IEEE International Power Electronics and Application Conference and Exposition (PEAC) in 2018. He received the Chinese Government Award for Outstanding Self-Financed Students Abroad in 2018 and the Best Thesis Award from NTU in 2019. He has published two ESI highly cited papers.



Han Deng (S'17) received the B.Eng. degree in electrical engineering from Xi'an Jiaotong University, Xi'an, China, in 2017 and the M.Sc. degree in power engineering from Nanyang Technological University, Singapore, in 2018, respectively. She is currently working towards the Ph.D. degree at Nanyang Technological University, Singapore. Her research interests include modeling, stability analysis, and control of distributed generation in more-electronics power systems.



Stefan M. Goetz (M'14) received his undergraduate and graduate degrees from TU Muenchen, Germany. He obtained doctoral training at TU Muenchen as well as Columbia University and received the PhD degree in 2012 with a thesis on medical applications of power electronics for which he was awarded a PhD thesis prize from TU Muenchen.

Dr. Goetz is currently on faculty at Duke University and TU Kaiserslautern. His research interests include precise high-power pulse synthesizers for magnetic neurostimulation and noninvasive brain stimulation as well as integrative power electronics solutions for microgrids and electric vehicle applications.